Capacitance of the Abrupt Transition from Coaxial-to-Circular Waveguide

M. RAZAZ AND J. BRIAN DAVIES, MEMBER, IEEE

Abstract—**A least-squares boundary residual method is applied to calculate the discontinuity capacitance of an abrupt transition from coaxial-to-circular waveguide. Accurate values of the capacitance are presented here and compared with published results. Our results are believed to be accurate to about ±0.1 fF and hence suitable for standards work.**

I. Introduction

IN THIS WORK, the least-squares boundary residual method (LSBRM) is applied to study a coaxial open-circuit junction, as in Fig. 1. LSBRM is a numerical technique which has attracted attention only recently [9], [17], [18], [20]–[22]. An accurate knowledge of the discontinuity capacitance [1] assumes the greatest importance in the measurement of very small values of capacitance and in immittance standardization [2].

The junction has been investigated by a number of authors. Whinnery and Jamieson [1] were the first to study the step transition of the junction and justify the concept of an equivalent shunt capacitance placed at the plane of the discontinuity. In a subsequent paper, Whinnery *et al.* [3] evaluated the effects of discontinuities in coaxial lines using Hahn's series approach, and presented the values of the discontinuity capacitance for different junctions in the form of graphs. Later investigations have shown that the original charts were in error by up to 5 percent [4], and were thus not suitable for standards work. Somlo [4], [5] recomputed the equations derived by Whinnery *et al.* [3] to five significant digits, thus presenting more accurate results for the discontinuity capacitance than had been available before. Risley [6], [7] found the upper and lower bounds to the capacitance using a Rayleigh–Ritz variational method. The advantage of this technique is that it is mathematically rigorous. If proper formulations for the upper and lower bounds can be found, it provides an error estimation to the capacitance, and hence the termination may be used for standards work. The main disadvantages of the technique are that, for the analysis and computer programming, it needs two separate, lengthy formulations for the calculation of the upper and lower bounds; and numerical truncation and round-off errors will invalidate the strictness of the bounds. Woods [8], by interpolation of Somlo's data [4] has calculated the values of the discontinuity capacitance for different coaxial line dimensions to four significant digits. However, Woods' and Somlo's results differ significantly from those obtained by Risley [6], [7], and are closer to measured values [8].

Manuscript received May 23, 1977; revised August 4, 1978.

The authors are with the Department of Electronic and Electrical Engineering, University College, Torrington Place, London, England.

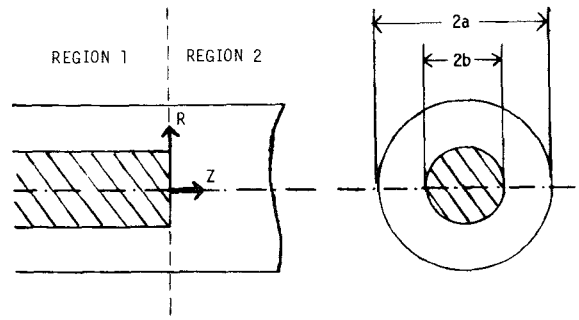

Fig. 1. Coaxial open-circuit junction.

Jurkus [19], following Somlo's work [4], [5] closely has recomputed the capacitance of discontinuities formed by coplanar-transverse steps in conductors of a coaxial line as in [3]. For the case of abrupt transitions, as in this paper, Jurkus claims results for the discontinuity capacitance that agree with Somlo's published results to within 0.05 percent, although without presenting any numerical values.

Therefore, from both the theoretical and practical points of view, more accurate results for the discontinuity capacitance are needed. The purpose of this work is to demonstrate the successful application of LSBRM to this problem, and to report accurate values obtained for the discontinuity capacitance of the open-circuited junction (see Fig. 1) with different line dimensions. These results are believed to be accurate to ±0.1 fF, and thus usable for standards work. No such accuracy has been reported before. For more detail on the work described in this paper [17] should be consulted. An outline of earlier results of this work was given in [18].

II. Field Analysis

Consider the abrupt junction of a lossless coaxial-to-circular waveguide as in Fig. 1. We assume that the device is excited by an incident TEM wave which travels in region 1 ($z<0$) towards the junction at $z=0$, and that the output circular guide is of infinite length, with a diameter such that all modes in region 2 ($z>0$) are evanescent.

Owing to the junction discontinuity, a reflected TEM wave plus an infinite number of TM_{0n} coaxial waveguide modes in region 1, and an infinite number of circular

0018-9480/79/0600-0564$00.75 ©1979 IEEE

TM_{0m} modes in region 2 are excited. As a result of symmetry, all the modes excited have fields that are independent of θ, and evanescent TE modes cannot be excited in either region.

Combining expressions for the transverse components of the TEM and TM modes, we can write the expressions for the total transverse fields in the coaxial line ($z<0$) as follows:

$$E_r^{(1)} = a_0\psi_0(e^{-\gamma_0 z} + \rho e^{+\gamma_0 z}) + \sum_{n=1}^{\infty} a_n\phi_n e^{+\gamma_n z} \tag{1}$$

$$H_\theta^{(1)} = \eta_0 a_0\psi_0(e^{-\gamma_0 z} - \rho e^{+\gamma_0 z}) - \sum_{n=1}^{\infty} \eta_n a_n\phi_n e^{+\gamma_n z} \tag{2}$$

where $\rho = a_0'/a_0$ is the required reflection coefficient at the junction ($z=0$), a_0 and a_0' being the amplitudes of the incident and reflected TEM modes, respectively; ϕ_n, γ_n, and η_n denote, respectively, the normalized mode functions, propagation constants, and wave admittances for TM coaxial waveguide modes; ψ_0, γ_0, η_0 are the corresponding quantities for the TEM modes. The expressions for all these quantities are given in [17].

Similarly, in the circular waveguide region ($z>0$), we have as expressions for the total transverse fields

$$E_r^{(2)} = \sum_{m=1}^{\infty} b_m\phi_m' e^{-\gamma_m' z} \tag{3}$$

$$H_\theta^{(2)} = \sum_{m=1}^{\infty} \eta_m' b_m\phi_m' e^{-\gamma_m' z} \tag{4}$$

where ϕ_m', γ_m', and η_m' concern the TM circular waveguide modes [17].

From (1) to (4), we proceed to match the transverse fields across the boundary ($z=0$) between the regions by using LSBRM. The boundary residual [9], [17] at the junction can be represented by a positive-definite Hermitian form in the amplitude coefficients as

$$\begin{aligned} I(a_0, a_0', \{a_n\}, \{b_m\}) &= \boldsymbol{\alpha}^{*T}\boldsymbol{F}\boldsymbol{\alpha} \\ &= \int_S \left(|E_t^i - E_t^j|^2 + pZ_0^2|H_t^i - H_t^j|^2\right) W(s)\,ds \\ &= \int_b^a 2\pi\left(|E_r^{(1)} - E_r^{(2)}|^2 + pZ_0^2|H_\theta^{(1)} - H_\theta^{(2)}|^2\right) r\,dr \\ &\quad + \int_0^b 2\pi|E_r^{(2)}|^2 r\,dr \end{aligned} \tag{5}$$

where $W(s)$ is an arbitrary weighting function, subsequently put to unity:

$$\boldsymbol{\alpha}^T = (a_0, a_0', \{a_n\}, \{b_m\}) \tag{6}$$

and p is a dimensionless scaling factor, Z_0 is the free-space wave impedance; and the various components of the E and H fields are found from (1) to (4) by putting $z=0$. In order to precisely match the fields across the boundary at $z=0$, the field residuals, and hence the Hermitian form of (5) must vanish. To achieve this, an infinite number of modes must be included in the equation. However, for numerical purposes we truncate the number of modes in the field expansions, and require that the Hermitian form of (5) be minimized for a given amplitude of incident TEM wave. This minimization, according to [9] is given by

$$\boldsymbol{C}\boldsymbol{x} = \boldsymbol{v} \tag{7}$$

resulting in the minimum value

$$\lambda_1 = v_0 - \boldsymbol{v}^{*T}\boldsymbol{x} \tag{8}$$

where the matrix $\boldsymbol{F}$ of (5) is partitioned as

$$\boldsymbol{F} = \left(\begin{array}{c|c} v_0 & \boldsymbol{v}^{*T} \\ \hline \boldsymbol{v} & \boldsymbol{C} \end{array}\right) \tag{9}$$

and

$$\boldsymbol{x}^T = \left(\rho, \left\{\frac{a_n}{a_0}\right\}, \left\{\frac{b_m}{a_0}\right\}\right). \tag{10}$$

Summarized expressions are given in the Appendix for the matrix elements of $\boldsymbol{F}$ above. Therefore, the problem of minimizing (5) is reduced to solving (7), the solution of which gives in $\boldsymbol{x}$ the required reflection coefficient ρ, and the approximate coefficients $\{a_n\}$ and $\{b_m\}$.

Now having obtained ρ, the normalized input admittance y_{in} of Fig. 1 can be found from

$$y_{in} = \frac{1-\rho}{1+\rho}. \tag{11}$$

The discontinuity capacitance C_d is then given by

$$C_d = \frac{Y_c}{\omega}\,\mathrm{Im}\,(y_{in}) \tag{12}$$

where Y_c is the characteristic admittance of the coaxial line, and is given by

$$Y_c = \frac{\sqrt{\epsilon_r}}{60}\,\frac{1}{\log(a/b)}.$$

An advantage of the least-squares method is that it is concerned with a positive (semi-) definite system, in that an error residual is being minimized which is by definition real and nonnegative. If the matrix order is increased for a given problem, the boundary residual is easily calculated, and a typical plot is shown in Fig. 2. The curves are for different values of the scaling factor p, defined in (5). This plot is a valuable check on convergence, as reduction of the Hermitian form residual to zero is sufficient, as well as a necessary condition.

The main advantages of the LSBRM technique for this discontinuity problem are [9], [17]: 1) rigorous convergence, being free from problems of relative convergence, 2) the error minimization being global rather than discrete, as in the case of point matching, 3) the use of, probably, the fastest matrix solution algorithm, namely Choleski's method without pivoting: 4) the flexibility of the scaling factor p in producing the generally decreasing upper bounds and increasing lower bounds with variable degrees of convergence. It was found [17] that particular care had to be taken with the round-off and truncation errors by proper formulation of the matrix elements, otherwise the matrix $\boldsymbol{C}$ becomes nonpositive-definite and

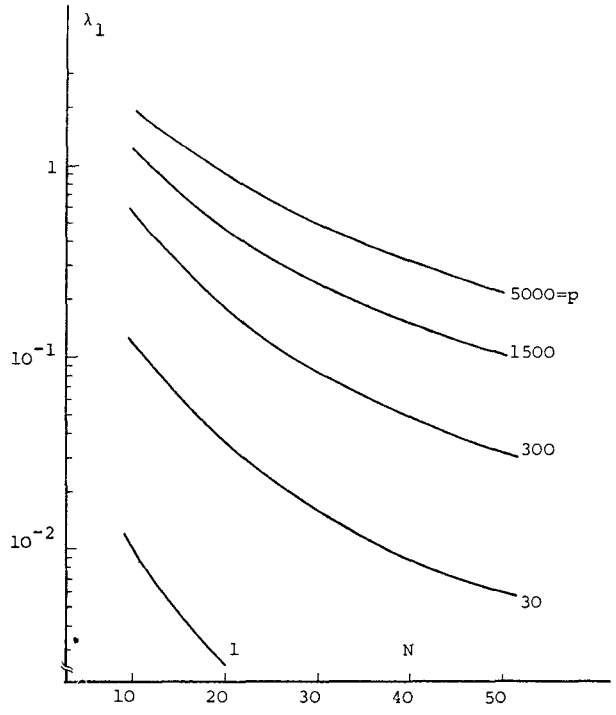

Fig. 2. Minimum of Hermitian form against number of modes.

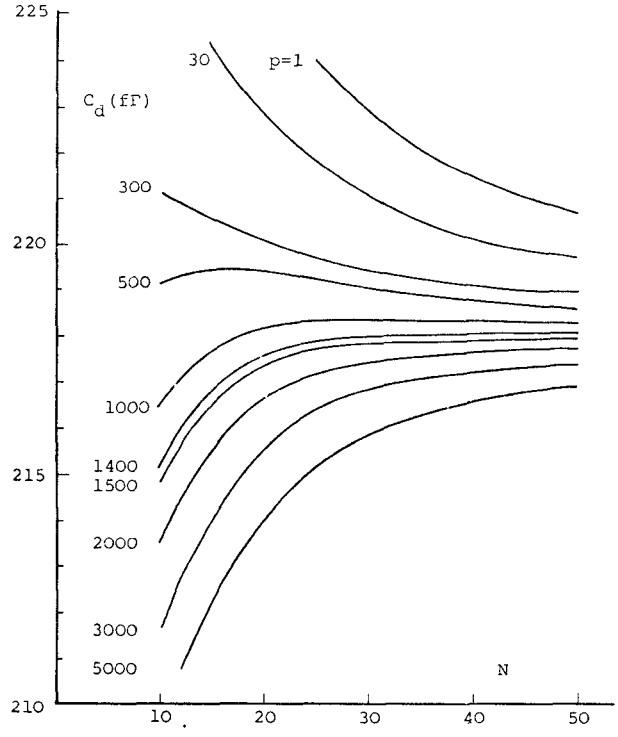

Fig. 3. Equivalent capacitance against number of modes.

the method fails to produce correct results. In this respect a significant improvement in the accuracy of the results was achieved by using 1) highly accurate values of the Bessel functions and their roots, and 2) by improved formulation of the inner products (see Appendix) with maximum use of the orthogonality relations. For instance, use of Bessel functions and their roots, accurate only to five significant figures, was found to make the curves in Fig. 2 deviate wildly, and matrix $\boldsymbol{C}$ to even go nonpositive-definite at orders around 10. By contrast, using the corresponding values accurate to fifteen significant figures in conjunction with the improved formulation gave smooth curves as in Fig. 2 with matrix orders of up to 100. It was also found [17] that numerical integration of the elements of matrix $\boldsymbol{F}$ should be avoided if at all possible, because of the difficulty of achieving adequate accuracy.

III. Numerical Results

To solve (7), Cholesky's method with iterative refinement [10] was used, and so gave an estimated P-condition number of matrix $\boldsymbol{C}$ [11].

As a first example, for the calculation of discontinuity capacitance, a 50-Ω 3/4-in (19.05-mm) open-circuited vacuum coaxial line with solid inner conductor was studied. The inner and outer dimensions of the line are $2b = 8.2723 \pm 0.0005$ mm and $2a = 19.0487 \pm 0.0005$ mm, respectively. The reasons for choosing this particular line were twofold. Firstly, upper and lower bounds to the corresponding discontinuity capacitance have been evaluated by Risley, using the Rayleigh–Ritz variational method [6], [7]; secondly, the measured value of the capacitance is available [6].

These upper and lower bounds and the measured value, at 1000 Hz, are 217.7, 215, and 216.4 ± 1 fF, respectively. Fig. 3 shows the results for the discontinuity capacitance C_d against the mode number N at $f = 1$ GHz with different values of the scaling factor p defined in (5). The number of modes on each side of the discontinuity can be selected independently, as the Hermitian form of (5) always has a minimum. In contrast to both point-matching and Fourier-mode matching, which are critically dependent on some point selection or number of terms in a kernel approximation [12], [13], it was found that altering the ratio $M:N$ did not affect the apparent limit of convergence; thus $N = M$ was used for Fig. 3.

Fig. 3 also shows that the smaller values of the scaling factor p correspond to a generally decreasing upper bound, and conversely for the larger values. This dependence of convergence from above or below, which is a distinct advantage of LSBRM, is taken to be directly related to Schwinger's variational bounds [14], [15]; the extreme values of p are associated with greater weighting to the electric or magnetic boundary residuals (see 5).

An appropriate criterion for the selection of optimum p would be to minimize the slope $(\partial C_d)/(\partial N)$ of Fig. 3. This means that with a small (but not too small) value of N, say $N = 20$, the optimum scaling factor p_{opt} can be approximated. Then as N is increased, the exact solution can be approached with the most suitable convergence, and hence, the possibility of a large saving of computer time.

Fig. 4 illustrates the P-condition number of matrix $\boldsymbol{C}$ (for the case shown in Fig. 3) against the scaling factor p for different matrix orders. It is interesting to note that the minimum value of the condition number occurs for a

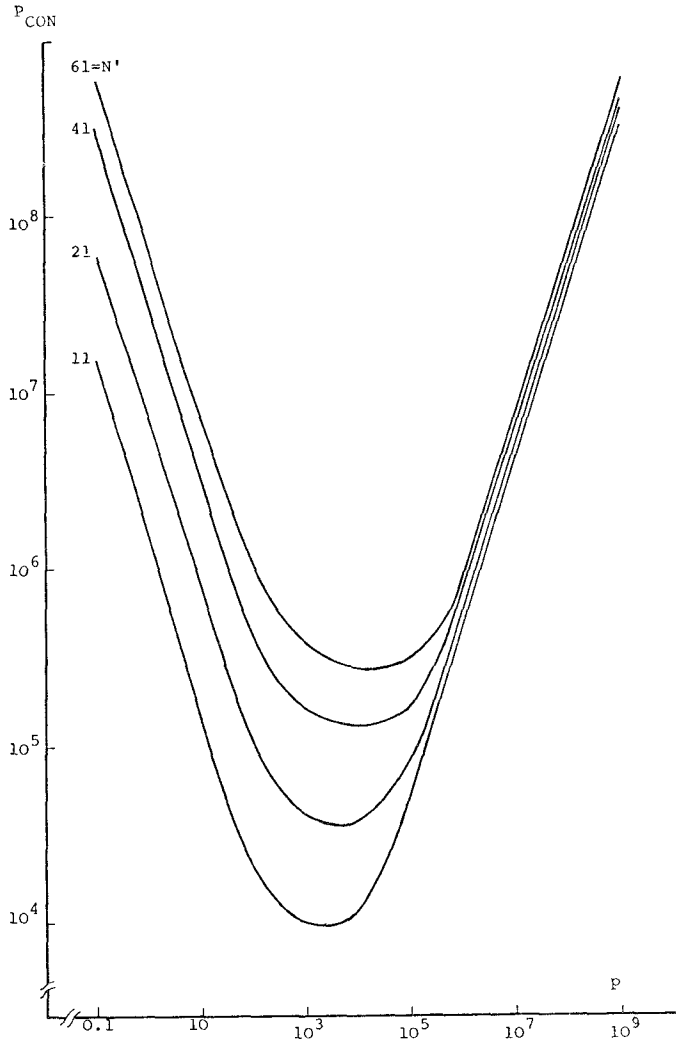

Fig. 4. *P*-condition number of C against scaling factor p for different matrix orders N'.

range of scaling factors close to that for optimum convergence (see Fig. 3). We believe that an evaluation of the matrix condition number is a most desirable check on the numerical stability of the solution.

Table I shows values of the discontinuity capacitance C_d computed by different authors for the coaxial open-circuit junction of Fig. 1 with different line sizes. Table II represents the percentage difference of the results (from Table I) with respect to each other.

From these Tables one can see that our results, in general, agree to within 0.17 to 0.25 percent with Woods' and Somlo's results, which in turn are close to the measured values [5], [8].

For both the 7-mm (50-Ω) line and the 19.05-mm (50-Ω) line, Risley's results are approximately 1 percent higher than ours, while for the 14-mm (50-Ω) line, his result is 2.9 percent higher. In contrast, for the 19.05-mm (24.3-Ω) line, Risley's results are about 3 percent lower than ours (see Table II).

We should note that in Table I of Risley's paper [6], the value of the characteristic impedance for the 19.05-mm ($a/b=1.5$) line should read 24.3 Ω instead of 25.3 Ω. For this case, however, our much higher result for the capacitance and the result given by Woods (see Table I) are consistent with the measured value of 396±2.0 fF obtained by Spinney [8]. For the case of the 19.0487-mm (50-Ω) line, Risley's result for the upper bound is, surprisingly, only 0.15 percent higher than ours.

The 14.2875-mm (50-Ω) line in Table I was specifically chosen to compare our results with Woods' results and also, with the measured value of 162.4±0.5 fF given by Zorzy [8]. These comparisons show that there is good agreement between Woods' results and ours, which in turn, support the measured value to within the experimental error.

We note that in Table I, our computed value of each capacitance for given termination and frequency is the average value of the most accurate upper and lower bounds with appropriate scaling factors.

We believe that our results for the discontinuity capacitance are accurate to about ±0.1 fF, and hence, suitable for standards work. This kind of accuracy is obtainable with a typical number of modes, $N=M=50$.

Appendix
Formulation of the Elements of F

Substituting E_r and H_θ from (1) to (4) into (5) gives

$$\boldsymbol{\alpha}^{*T}\boldsymbol{F}\boldsymbol{\alpha}=\int_b^a 2\pi\left|(a_0+a_0')\psi_0+\sum_{n=1}^{N}a_n\phi_n-\sum_{m=1}^{M}b_m\phi_m'\right|^2 r\,dr$$
$$+pZ_0^2\int_b^a 2\pi\left|(a_0-a_0')\psi_0\eta_0-\sum_{n=1}^{N}a_n\eta_n\phi_n-\sum_{m=1}^{M}b_m\eta_m'\phi_m'\right|^2 r\,dr$$
$$+\int_0^b 2\pi\left|\sum_{m=1}^{M}b_m\phi_m'\right|^2 r\,dr. \tag{13}$$

We now partition C and v of (7) as

$$\boldsymbol{C}=\begin{bmatrix} C_{11} & C_{12} & C_{13} \\ & C_{22} & C_{23} \\ U_c^{*T} & & C_{33}\end{bmatrix} \tag{14}$$

$$v^T=(v_1,g_N^T,h_M^T) \tag{15}$$

where U_c is the upper triangle of C.

The evaluation of (13) is lengthy and involves inner products of Bessel functions of the first and second kinds. However, the choice of the weighting function $W(s)=1$ makes the inner products expressible in terms of Lommel integrals [16], and hence, offers the possibility of finding closed form solutions for the elements of F. In formulating these elements, care has been taken to minimize effects of the corresponding round-off errors. The analytical formulas derived for the elements of F not only avoid approximation errors inherent in any numerical integration, but also provide ease of computation. To avoid lengthy details, only the final formulas are presented in the following:

$$v_0=\langle\psi_0,\psi_0\rangle(1+p)\qquad v_1=\langle\psi_0,\psi_0\rangle(1-p) \tag{16}$$

$$g_N(n)=0\qquad h_M(m)=-\langle\psi_0,\phi_m'\rangle(1+p'\eta_0\eta_m') \tag{17}$$

TABLE I
VALUES OF DISCONTINUITY CAPACITANCE FOR COAXIAL OPEN-CIRCUIT JUNCTION OF DIFFERENT SIZES

LINE SIZE		FREQUENCY	RISLEY'S UPPER BOUND RESULTS	SOMLO'S RESULTS	WOODS' RESULTS	RAZAZ AND DAVIES' RESULTS
2a (mm)	Z_c (Ω)	f (Hz)	C_d (fF)	C_d (fF)	C_d (fF)	C_d (fF)
7	50	10^3	80.66	79.70	79.7	79.88
		10^9	80.70	* (not available)	79.7	79.917
14	50	10^3	164.56	159.40	159.4	159.76
		10^9	164.85	*	*	160.039
14.2875	50	10^3	*	162.67	162.7	163.04
		10^9	*	*	163.0	163.336
19.05	50	10^3	219.49	216.89	217.0	217.40
		10^9	220.18	*	217.7	218.07
(NBS) 19.0487 ± .0005	50	10^3	217.71	216.88	216.9557	217.38
		10^9	*	*	*	218.05
19.05	24.3	10^3	386.51	*	398.8	399.02
		10^9	387.68	*	*	400.18

TABLE II
RELATIVE DIFFERENCES (IN PERCENTAGE) OF DIFFERENT RESULTS FOR DISCONTINUITY CAPACITANCE

LINE SIZE		FREQUENCY	RISLEY'S RESULTS w.r.t. WOODS'	RISLEY'S RESULTS w.r.t. RAZAZ DAVIES'	RAZAZ DAVIES' RESULTS w.r.t. WOODS'	RAZAZ DAVIES'S RESULTS w.r.t. SOMLO'S
2a (mm)	Z_c (Ω)	f (Hz)	% Difference	% Difference	% Difference	% Difference
7	50	10^3	1.19	0.97	0.22	0.22
		10^9	1.24	0.99	0.25	*
14	50	10^3	3.13	2.92	0.22	0.22
		10^9	*	2.92	*	*
14.2875	50	10^3	*	*	0.21	0.23
		10^9	*	*	0.21	*
19.05	50	10^3	1.13	0.95	0.18	0.23
		10^9	1.13	0.96	0.17	*
(NBS) 19.0487 ±.0005	50	10^3	0.35	0.15	0.20	0.23
		10^9	*	*	*	*
19.05	24.3	10^3	-3.18	-3.24	0.05	*
		10^9	*	-3.22	*	*

*not available

$$C_{11}=v_0 \qquad C_{12}(1,n)=0 \tag{18}$$

$$C_{13}(1,m)=\langle\psi_0,\phi'_m\rangle(-1+p'\eta_0\eta'_m) \tag{19}$$

$$C_{22}(n,i)=\langle\phi_n,\phi_i\rangle(1+p'\eta_n^*\eta_i)\delta_{ni} \tag{20}$$

$$C_{23}(n,m)=\langle\phi_n,\phi'_m\rangle(-1+p'\eta_n^*\eta'_m) \tag{21}$$

$$C_{33}(m,j)=-\langle\phi'_m,\phi'_j\rangle^{(0,b)}(p'\eta'_m{}^*\eta'_j)+\gamma'^2_m(1+p'\eta'_m{}^*\eta'_j)\delta_{mj} \tag{22}$$

$$\delta_{ij}=\begin{cases}1, & i=j \quad m,j=1,2,\cdots,M\\ 0, & i\neq j \quad n,i=1,2,\cdots,N\end{cases}$$

where $p'=pZ_0^2$, δ_{ij} is the Kronecker delta, and the symbol $\langle,\rangle$ shows an inner product over the aperture, unless it is otherwise specified.

The expressions for the inner products in (16)–(22) are

$$\langle\psi_0,\psi_0\rangle=K_0^2 \tag{23}$$

$$\langle\psi_0,\phi'_m\rangle=2\pi c_0 c_m\frac{\gamma'_m}{K'^2_m}J_0(K'_m b) \tag{24}$$

$$\langle\phi_n,\phi_i\rangle=\pi\gamma_n^2K_n^2\left[a^2R_1^2(K_n a)-b^2R_1^2(K_n b)\right]\delta_{ni} \tag{25}$$

$$\langle\phi_n,\phi'_m\rangle=2\pi bc_m\frac{\gamma_n\gamma'_m K_n}{K'^2_m-K_n^2}J_0(K'_m b)R_1(K_n b) \tag{26}$$

$$\langle\phi'_m,\phi'_j\rangle^{(0,b)}=\left[\frac{\gamma'_{mb}}{aJ_1(K'_m a)}\right]^2\cdot\left[J_1^2(K'_m b)-J_0(K'_m b)J_2(K'_m b)\right]\delta_{mj}+C'_2(1-\delta_{mj})\left[(K'_j b)J_0(K'_j b)J_1(K'_m b)-(K'_m b)J_0(K'_m b)J_1(K'_j b)\right] \tag{27}$$

where c_m, C'_2, and $R_1(K_n r)$ are given by

$$c_m=\frac{K'_m}{\sqrt{\pi}\,aJ_1(K'_m a)} \tag{28}$$

$$C'_2=\frac{2}{a^2}\frac{\gamma'_j\gamma'_m}{K'^2_m-K'^2_j}\frac{1}{J_1(K'_j a)J_1(K'_m a)} \tag{29}$$

$$R_1(K_n r)=A_1J_1(K_n r)+B_1Y_1(K_n r). \tag{30}$$

One interesting feature of (16)–(22) is that all elements of $\boldsymbol{F}$ have physical interpretations in terms of the TEM and TM modes in Fig. 1. As an example, v_1 represents the contribution from the incident and reflected TEM modes; and the elements of, say $\boldsymbol{C}_{23}$, show the contributions from the evanescent TM modes in the coaxial and waveguide regions, and so on.

It should be noted that (23) is the same as equation (38) in [6]. In equation (44) of [6] there is a misprint, where $(y'_n)^2$ in the denominator must be replaced by γ'^2_n of Risley's notation. When this is done it becomes identical to (24) of this paper. There is, however, considerable difference between (25) and (26) here and their counterparts in [6] given by their equations (45)–(51). These inner products have been independently tested and compared [17], and it was found that the formulations used here are far less prone to round-off errors (and use less computer time). The significant improvement is essentially due to the greater use of orthogonality relations in our formulations, so that all the Bessel function products of type J_0J_2, Y_0Y_2, J_0Y_2, and Y_0J_2 present in equations (45)–(51) of [6] are absent from (25) and (26). There is no counterpart formulation in [6] to the inner product $\langle\phi'_m,\phi'_j\rangle$ of (27).

References

[1] J. R. Whinnery and H. W. Jamieson, "Equivalent circuits for discontinuities in transmission lines," *Proc. IRE*, vol. 32, pp. 98–115, Feb. 1944.

[2] R. N. Jones and L. E. Huntley, "Precision coaxial connectors in lumped parameter immittance measurements," *IEEE Trans. Instrum. Meas.*, vol. IM-15, pp. 375–380, Dec. 1966.

[3] J. R. Whinnery, H. W. Jamieson, and T. E. Robbins, "Coaxial line discontinuities," *Proc. IRE*, vol. 32, pp. 695–709, Nov. 1944.

[4] P. I. Somlo, "The discontinuity capacitance and the effective position of a shielded open circuit in a coaxial line," *Proc. IRE* (Australia), vol. 28, pp. 7–9, Jan. 1967.

[5] ——, "The computation of coaxial line step discontinuities," *IEEE Trans. Microwave Theory Tech.*, vol. MTT-15, pp. 48–52, Jan. 1967.

[6] E. W. Risley, "Discontinuity capacitance of a coaxial line terminated in a circular waveguide," *IEEE Trans. Microwave Theory Tech.*, vol. MTT-17, pp. 86–92, Feb. 1969.

[7] ——, "Discontinuity capacitance of a coaxial line terminated in a circular waveguide: Part II—Lower bound solution," *IEEE Trans. Microwave Theory Tech.*, vol. MTT-21, pp. 564–566, Aug. 1973.

[8] D. Woods, "Shielded-open-circuit discontinuity capacitance of a coaxial line," *Proc. Inst. Elec. Eng.*, vol. 119, pp. 1691–1692, Dec. 1972.

[9] J. B. Davies, "A least-squares boundary residual method for the numerical solution of scattering problems," *IEEE Trans. Microwave Theory Tech.*, vol. MTT-21, pp. 99–104, Feb. 1973.

[10] G. E. Forsythe and C. B. Moler, *Computer Solution of Linear Algebraic Systems*. Englewood Cliffs, NJ: Prentice Hall, 1967.

[11] J. R. Westlake, *A Handbook of Numerical Matrix Inversion and Solution of Linear Equations*. New York: Wiley, 1968, pp. 88–91.

[12] S. W. Lee, W. R. Jones, and J. J. Campbell, "Convergence of numerical solutions of iris-type discontinuity problems," *IEEE Trans. Microwave Theory Tech.*, vol. MTT-19, pp. 528–536, June 1971.

[13] R. Mittra, "On the fundamental limitation of numerical solution of integral equations," presented at the URSI Spring Meeting, Washington, DC, Apr. 1972.

[14] J. Schwinger and D. S. Saxon, *Discontinuities in Waveguides*. New York: Gordon & Breach, pp. 57–97, 1968.

[15] E. L. Chu and W. W. Hansen, "Disk loaded waveguides," *J. Appl. Phys.*, vol. 20, pp. 280–285, 1949.

[16] F. E. Relton, *Applied Bessel Functions*. London: Blackie, 1949.

[17] M. Razaz, "Computer solution of waveguide problems by least-squares boundary residual and mode matching methods," Ph.D. Dissertation, Dep. Electron. and Elec. Eng., Univ. College, London, England, 1976.

[18] M. Razaz and J. B. Davies, "Admittance of a coaxial-to-circular waveguide junction," *Electron. Lett.*, vol. 10, pp. 324–326, July 1974.

[19] A. Jurkus, "Computation of step discontinuities in coaxial line," *IEEE Trans. Microwave Theory Tech.*, vol. MTT-20, pp. 708–709, Oct. 1972.

[20] H. Oraizi and J. Perini, "A numerical method for the solution of the junction of cylindrical waveguides," *IEEE Trans. Microwave Theory Tech.*, vol. MTT-21, pp. 640–642, 1973.

[21] R. Jansen, "On the performance of the least-squares method for waveguide junctions and discontinuities," *IEEE Trans. Microwave Theory Tech.*, vol. MTT-23, pp. 434–436, 1975.

[22] H. J. A. LaRiviere and J. B. Davies, "The solution of electromagnetic eigenvalue problems by least-squares boundary residuals," *IEEE Trans. Microwave Theory Tech.*, vol. MTT-23, pp. 436–441, 1975.